

## Boundary Conditions Generated by Dynamic Particles in SPH Methods

A. J. C. Crespo<sup>1</sup>, M. Gómez-Gesteira<sup>1</sup> and R. A. Dalrymple<sup>2</sup>

**Abstract:** Smoothed Particle Hydrodynamics is a purely Lagrangian method that can be applied to a wide variety of fields. The foundation and properties of the so called dynamic boundary particles (DBPs) are described in this paper. These boundary particles share the same equations of continuity and state as the moving particles placed inside the domain, although their positions and velocities remain unaltered in time or are externally prescribed. Theoretical and numerical calculations were carried out to study the collision between a moving particle and a boundary particle. The boundaries were observed to behave in an elastic manner in absence of viscosity. They allow the fluid particles to approach till a critical distance depending on the energy of the incident particle. In addition, a dam break confined in a box was used to check the validity of the approach. The good agreement between experiments and numerical results shows the reliability of DBPs.

**Keyword:** Meshfree methods, SPH, smoothed particle hydrodynamics, boundary conditions

### 1 Introduction

Smoothed Particle Hydrodynamics, SPH, is a purely Lagrangian method developed during seventies [Lucy (1977); Gingold and Monaghan (1977)] to avoid some of the limitations of finite difference methods. The numerical method has been shown to be robust and applicable to a wide variety of fields. It has been successfully used in astrophysical applications [Gingold and Monaghan (1977)] and hydrodynamical problems as the study of gravity currents [Monaghan (1996); Monaghan, Cas, Kos and Hallworth (1999)], free

surface flows, specially wave propagation [Monaghan (1994); Monaghan and Kos [1999]; Monaghan and Kos (2000)] and solid simulation [Benz and Asphaug, (1994); Benz and Asphaug (1995); Vignjevic, De Vuyst and Campbell (2006)]. Recently, SPH has been used for wave impact studies on offshore structures [Dalrymple, Knio, Cox, Gómez-Gesteira and Zou (2002); Gómez-Gesteira and Dalrymple (2004); Gómez-Gesteira, Cerqueiro, Crespo and Dalrymple (2005); Crespo, Gómez-Gesteira and Dalrymple (2007a)].

The main advantages of SPH come from its purely Lagrangian nature. The method can easily deal with the existence of large voids without a special treatment and prevent the appearance of grid generating numerical diffusion. In addition the method can handle large deformations from the initial configuration and permits the description of complex media where the substance under scope (e.g.. star gas, fluid or solid) can be splitted into multiple connected regions, which can eventually recover their continuous nature without need of sophisticated and rather unphysical approaches. From a numerical point of view, the method can be used in a 1D, 2D or 3D configuration with little effort. Finally, multiphase media (e.g. liquid-gas or fluids with different densities) can also be described by the method.

In the particular case of fluids, SPH integrates the dynamical equations of motion for each particle in the Lagrangian formalism. It computes the relevant physical quantities for each particle as an interpolation of the values of the nearest neighboring particles, and then moves the particles according to those values.

The foundation of SPH is interpolation theory. The conservation laws of continuum fluid dynamics, in the form of partial differential equations, are transformed into integral equations through

<sup>1</sup> Grupo de Física de la Atmósfera y del Océano, Facultad de Ciencias, Universidad de Vigo, Spain.

<sup>2</sup> Department of Civil Engineering, Johns Hopkins University, Baltimore, USA.

the use of an interpolation function that gives the kernel estimate of the field variables at a point. Computationally, information is known only at discrete points, so that the integrals are evaluated as sums over neighboring points.

Since the first applications of the SPH method to hydrodynamical problems considerable effort has been devoted to the boundary conditions. Actually, the boundaries are constituted by particles that exert repulsive forces on fluid particles. Thus, central forces are a natural choice [Monaghan (1992)]. Nevertheless, the same author found that a better approach can be obtained by means of an interpolation procedure, in such a way that the force exerted is normal to the boundary [Monaghan and Kos (1999)].

The aim of this manuscript is the study of the role of the so called Dynamic Boundary Particles (DBPs from now on). These particles share the same properties as the fluid particles. They follow the same equations of state and continuity, but they are not allowed to move or they move according to some external input.

## 2 The SPH method

The main features of the SPH method, which is based on integral interpolants, are described in detail in [Benz (1990); Monaghan (1982); Monaghan (1992); Liu (2003); Vignjevic, Reveles and Campbell (2006)] and we will only refer here to the representation of the constitutive equations in SPH notation. The key idea is to consider that a function  $A(r)$  can be approximated by

$$A(\vec{r}) = \int A(\vec{r}') W(\vec{r} - \vec{r}', h) d\vec{r}' \quad (1)$$

where  $h$  is the smoothing length. This approximation, in discrete notation, leads to:

$$A(\vec{r}) = \sum_b m_b \frac{A_b}{\rho_b} W_{ab} \quad (2)$$

where  $a$  and  $b$  are particles,  $m_b$  and  $\rho_b$  are mass and density respectively and  $W_{ab} = W(r_a - r_b, h)$  is the weight function or kernel.

### 2.1 Choice of weight function

Weight functions play a fundamental role in SPH method. They should be constructed following several conditions such as positivity, compact support, normalization, monotonically decreasing and delta function behavior [Benz (1990); Monaghan (1992); Liu (2003)]. A cubic spline kernel developed by Monaghan and Latanzio (1985) was used in our simulation:

$$W_{ab} = \frac{1}{\pi h^3} \begin{cases} 1 - \frac{3}{2}q^2 + \frac{3}{4}q^3 & \text{if } 0 \leq q \leq 1 \\ \frac{1}{4}(2-q)^3 & \text{if } 1 \leq q \leq 2 \\ 0 & \text{otherwise} \end{cases} \quad (3)$$

where  $q = r_{ab}/h$ , being  $r_{ab}$  the distance between particles  $a$  and  $b$ , and  $h$  the smoothing length in SPH. This smoothing length, often called influence domain or smoothing domain, controls the size of the area around particle  $a$  where contribution from the rest of the particles cannot be neglected. Other kernel choices as those described in Liu (2003) can be used with similar results.

Due to the particular choice of the cubic spline kernel, whose first derivative goes to zero with  $q$ , the tensile instability correction proposed by Monaghan (2000) was used to prevent particle clumping. In addition, the kernel was modified following the linear method proposed by Bonet and Kulasegaram (2000) in order to assure the normalization property, particularly near the free surface. Using this normalized cubic spline kernel, the basic equations of conservation can be represented in SPH notation as follows Monaghan (1992).

### 2.2 Momentum equation

Different approaches have been considered in SPH method to describe momentum equation due to the different formulations of the diffusive terms.

The artificial viscosity proposed by Monaghan (1992) has been classically used due to its simplicity. In SPH notation, the momentum equation can be written as

$$\frac{d\vec{v}_a}{dt} = - \sum_b m_b \left( \frac{P_b}{\rho_b^2} + \frac{P_a}{\rho_a^2} + \Pi_{ab} \right) \nabla_a W_{ab} + \tilde{\mathbf{g}} \quad (4)$$

where  $\vec{g}=(0, 0, -9.81)$  ms<sup>-2</sup> is the gravitational acceleration.

$\Pi_{ab}$  is the viscosity term:

$$\Pi_{ab} = \begin{cases} \frac{-\alpha \overline{c_{ab}} \mu_{ab} + \beta \mu_{ab}^2}{\overline{\rho_{ab}}} & \vec{v}_{ab} \vec{r}_{ab} < 0 \\ 0 & \vec{v}_{ab} \vec{r}_{ab} > 0 \end{cases} \quad (5)$$

with  $\mu_{ab} = h \vec{v}_{ab} \vec{r}_{ab} / \vec{r}_{ab}^2 + \eta^2$ , where  $\vec{r}_{ab} = \vec{r}_a - \vec{r}_b$  and  $\vec{v}_{ab} = \vec{v}_a - \vec{v}_b$ ; being  $\vec{r}_k$  and  $\vec{v}_k$  the position and the velocity corresponding to particle  $k$  ( $a$  or  $b$ );  $\overline{c_{ab}} = c_a + c_b / 2$ ,  $\eta^2 = 0.01h^2$ ,  $\alpha$  and  $\beta$  are parameters with different values according to each problem. Following Monaghan (1992),  $\beta$  will be considered to be zero.

### 2.3 Continuity equation

The fluid in the SPH formalism is treated as compressible, which allows using an equation of state to determine fluid pressure, rather than solving an equation. However, the compressibility is adjusted to slow the speed of sound so that the time step in the model (based on the speed of sound) is reasonable.

Changes in the fluid density were calculated by means of

$$\frac{d\rho_a}{dt} = \sum_b m_b \vec{v}_{ab} \vec{\nabla}_a W_{ab} \quad (6)$$

instead of using a weighted summation of mass terms [Monaghan (1992)], which leads to an artificial density decrease near fluid interfaces.

### 2.4 Equation of state

Following [Monaghan, Cas, Kos and Hallworth (1999); Batchelor (1974)], the relationship between pressure and density was assumed to follow the expression:

$$P = B \left[ \left( \frac{\rho}{\rho_0} \right)^\gamma - 1 \right] \quad (7)$$

where  $\gamma = 7$  and  $B = c_0^2 \rho_0 / \gamma$ , being  $\rho_0 = 1000$  kg m<sup>-3</sup> the reference density and  $c_0 = c(\rho_0)$ , the speed of sound at the reference density.

### 2.5 Moving the particles

Particles are moved using the XSPH variant due to Monaghan [Monaghan (1989)].

$$\frac{d\vec{r}_a}{dt} = \vec{v}_a + \varepsilon \sum_b \frac{m_b}{\overline{\rho_{ab}}} \vec{v}_{ab} W_{ab} \quad (8)$$

where  $\varepsilon=0.5$  and  $\overline{\rho_{ab}} = \rho_a + \rho_b / 2$ . This method moves the particle with a velocity that is close to the average velocity in its neighborhood.

### 2.6 Time stepping

The Verlet algorithm [Verlet (1967)] was used in our numerical simulations. The basic idea of the algorithm is to write two third-order Taylor expansions for the positions, one forward and one backward in time

$$\begin{aligned} \vec{r}(t + \Delta t) &= \vec{r}(t) + \vec{v}(t)\Delta t + (1/2)\vec{a}(t)\Delta t^2 \\ \vec{v}(t + \Delta t) &= \vec{v}(t) + 2 \cdot \vec{a}(t)\Delta t \end{aligned} \quad (9)$$

Time-step control involves the Courant condition, the force terms and the viscous diffusion term [Monaghan (1989)]. A variable time step  $\delta t$  was calculated according to Monaghan and Kos (1999):

$$\begin{aligned} \Delta t &= 0.3 \cdot \min(\Delta t_f, \Delta t_{cv}) \quad \Delta t_f = \min_a \left( \sqrt{h} / |f_a| \right) \\ \Delta t_{cv} &= \min_a \frac{h}{c_s + \max_b \left| \frac{h \vec{v}_{ab} \vec{r}_{ab}}{\vec{r}_{ab}^2} \right|} \end{aligned} \quad (10)$$

Here  $\Delta t_f$  is based on the force per unit mass  $\mathbf{f}$ , and  $\Delta t_{cv}$  combines the Courant and the viscous time-step controls.

### 2.7 Computational efficiency: neighboring list

Each particle of fluid needs a neighboring list inside a distance that will be the range of the Kernel,  $2h$  for cubic spline (see Figure 1). The whole list that is upgraded in each step of time requires  $N^2$  operations to calculate the interactions among all the couples of particles, where  $N$  is the particles amount.

In the code the computational domain is divided in square cells of  $2h$  side following Monaghan and

Latanzio (1985). Thus, for a particle located inside a cell, we only have to consider the interactions with the particles of neighboring cells. In this way the number of calculations for time step and, therefore, the computational time diminish considerably, from  $N^2$  operations to  $N \log N$

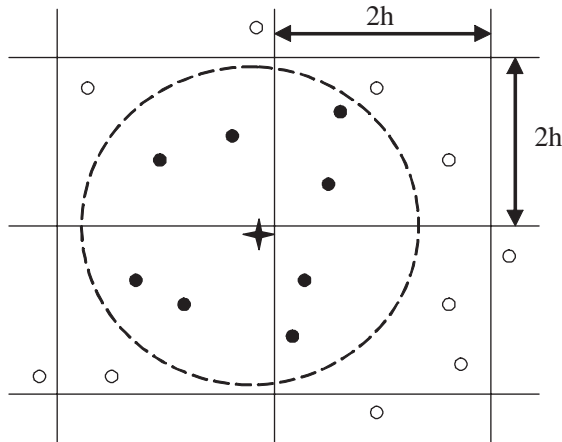


Figure 1: Set of neighboring particles. The particle marked with a star correspond to particle  $a$ . The possible neighbors in adjacent cells are marked with a dot. Particle  $a$  only interacts with particles inside the dashed circle (solid dots)

## 2.8 Boundary conditions

The boundary conditions do not appear in a natural way in the SPH formalism. When a particle approaches a solid frontier, in the summations (Eq. 1) only the particles located inside the system intervene without any interaction from the outside. This contribution can generate unrealistic effects, due to the different nature of the variables to solve, since some ones, as the velocity, fall to zero when they approach the boundaries, while others, as the density, not. The different solutions to avoid boundary problems consist on the creation of several virtual particles that characterize the system limits. Basically, three different types of particles can be distinguished:

**Ghost particles.** Randles and Libersky (1996) considered boundary particles whose properties, included their position, vary each time step.

When a real particle is close to a contour (at a distance shorter than the kernel smoothing length) then a virtual (ghost) particle is generated outside of the system, constituting the specular image of the incident one. Both particles have the same density and pressure, but opposite velocity. Thus, the number of boundary particles varies in each time step, which complicates its implementation in the code

**Repulsive particles.** This type of boundary particles is due to Monaghan (1994). In this case the particles that constitute the frontier exert central forces on the fluid particles, in analogy with the forces among molecules. Thus, for a boundary particle and a fluid particle separated a distance  $r$  the force for unit of mass has the form given by the Lennard-Jones potential. In a similar way, other authors [Peskin (1977)] express this force assuming the existence of forces in the boundaries, which can be described by a delta function. This method was refined in Monaghan and Kos (1999) by means of an interpolation process, minimizing the inter-spacing effect of the boundary particles on the repulsion force of the wall.

**Dynamic particles.** These particles verify the same equations of continuity and of state as the fluid particles, but their position remains unchanged or is externally imposed. An interesting advantage of these particles is their computational simplicity, since they can be calculated inside the same loops as fluid particles with a considerable saving of computational time. These particles were first presented in [Dalrymple and Knio, (2000)] and used in further studies on the interaction between waves and coastal structures [Gómez-Gesteira and Dalrymple (2004); Gómez-Gesteira, Cerqueiro, Crespo and Dalrymple (2005), Crespo, Gómez-Gesteira and Dalrymple (2007a)]. However, as far as we know, the properties of these particles have been not considered in detail.

### 3 Dynamic boundaries

#### 3.1 Repulsion Mechanism

The boundaries exert a force to the fluid particles when approaching. In order to analyze the fluid particles movement due to boundary particles, a schematic system composed by two particles, a boundary particle and a fluid one, was considered. The equation of state can be obtained from the first term of the Taylor expansion of Eq. (7), assuming that the speed of sound,  $c$ , is constant.

$$P_a = c^2(\rho_a - \rho_{a0}) \quad (11)$$

With  $a$  the moving particle and  $b$  the boundary one.

Considering the radial coordinate joining the center of both particles to coincide with an axis ( $Z$ ), the equation of motion (4) for the particle  $a$  (the fluid one) becomes

$$\frac{dv_a}{dt} = -m_b \left( \frac{P_b}{\rho_b^2} + \frac{P_a}{\rho_a^2} \right) \frac{\partial}{\partial z_a} W_{ab} \quad (12)$$

in absence of viscosity ( $\Pi_{ab}=0$ ) and gravity

Using Eq. (11) we obtain

$$\frac{dv_a}{dt} = -m_b c^2 \left( \frac{(\rho_b - \rho_0)}{\rho_b^2} + \frac{(\rho_a - \rho_0)}{\rho_a^2} \right) \frac{\partial}{\partial z_a} W_{ab} \quad (13)$$

The continuity equation can be written following Monaghan (1996)

$$\rho_a = \sum_b m_b W_{ab} \quad (14)$$

becoming

$$\rho_a = m_b W_{ab} + m_a W_{aa} \quad (15)$$

$$\rho_b = m_a W_{ab} + m_b W_{bb} \quad (16)$$

for the two particles under scope.

Being  $W_0 = W_{aa} = W_{bb} = W(r_{ab} = 0)$ . Assuming the same mass for both particles, the densities can be calculated following Eq. (15).

$$\rho_a = \rho_b = \rho = m(W_{ab} + W_0) \text{ and } \rho_0 = mW_0 \quad (17)$$

Thus Eq. (13) becomes

$$\frac{dv_a}{dt} = -2c^2 \frac{W_{ab}}{(W_{ab} + W_0)^2} \frac{\partial}{\partial z_a} W_{ab} \quad (18)$$

Considering the particular case of a Gaussian kernel [Monaghan (1982)]

$$W_{ab} = \frac{2\pi}{h} e^{-z_{ab}^2/h^2}, \quad \nabla W_{ab} = -\frac{2z_{ab}}{h^2} W_{ab}, \quad W_0 = \frac{2\pi}{h} \quad (19)$$

Eq. (18) becomes

$$\frac{dv_a}{dt} = \frac{4c^2}{h^2} z_{ab} \left( \frac{1}{1 + e^{z_{ab}^2/h^2}} \right)^2 \quad (20)$$

Thus, the direction of the force exerted on particle  $a$  by a boundary particle  $b$ , depends on the sign of  $z_{ab}$ . When the  $a$  approaches  $b$  from the above (below)  $z_{ab}$  becomes positive (negative) and, consequently, particle  $a$  is pushed up (down). Note that force tends to zero when  $z_{ab}$  tends to zero. This result is usually attained when using kernels whose first derivative goes to zero at  $z_{ab}$ . This effect can be prevented in numerical simulations using the tensile correction proposed by Monaghan (2000).

In general, the forces exerted on the moving particle can be summarized as

$$\frac{dv_a}{dt} = - \left( 2c^2 \frac{W_{ab}}{(W_{ab} + W_0)^2} + m\Pi_{ab} \right) \frac{\partial}{\partial z_a} W_{ab} - g \quad (21)$$

where the viscosity ( $\Pi_{ab}$ ) and gravity ( $g$ ) terms have been added. Note that Eq. (21) does not depend on a particular kernel definition. Actually, a Gaussian kernel was considered in Eq. (20) for mathematical simplicity, although a cubic spline kernel will be considered in further numerical simulations.

#### 3.2 Test problem 1: Particle movement inside a box

A simple test corresponding to the movement of a single particle inside a box was considered to depict the main features of the interaction between moving and boundary particles. In spite of the

schematic nature of the test, it proves that the particle can be kept inside the box due to the repulsive force without losses in the mechanical energy of the system.

Different tests were carried out with numerical model to study the evolution of a single particle inside a box (0.5×0.5 m). The boundary particles were placed in two rows forming a staggered grid as shown in Figure 2.

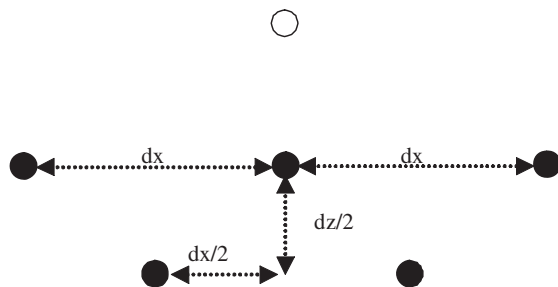


Figure 2: Sketch of the interaction between a fluid particle (empty circle) and a set of boundary particles (full circles). The boundary particles are placed in a staggered manner.

The separation between the boundary particles is  $dx = dz = h/1.3$  and  $h = 2.097 \cdot 10^{-2}m$ . In the Z axes the distance will be measured from the boundary particles. The first experiment was the fall of a particle from  $(X_0, Z_0) = (0.25, 0.3)$  m without initial velocity and zero viscosity ( $\alpha=0$ ). The particle was initially far from the boundaries, in such a way that gravity was the only initial force on the particle. This particle does not feel the interaction of the boundary particles until it approaches the bottom of the box. It is important to note that the boundary particle is situated exactly at the same X position as the moving particle, but at  $Z=0$ .

Figure 3 shows the repulsion mechanism. The incoming particle,  $a$ , increases the density locally (Fig. 3a) according to Eq.(6), which results in an increase in pressure following Eq.(7) (Fig. 3b) and in an increase of the pressure term  $(P/\rho^2)$  in Eq.(4). The normalized pressure term,  $NPT_z = (P/\rho^2)_z / (P/\rho^2)_R$ , is represented in Fig. 3c, where  $z$  refers to the distance from the incoming particle to the wall and  $R$  to the return point

of the incoming particle. Note how the fluid particle suffers the effect of the boundary when the distance particle boundary is shorter than  $2h$ .

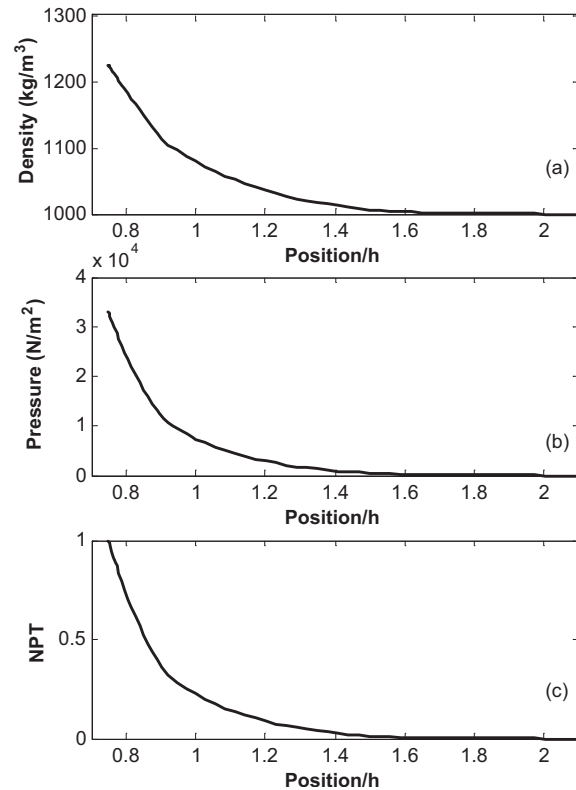


Figure 3: Variation of density (a), pressure (b) and normalized pressure term (c) for a moving particle approaching a solid boundary. Calculations were run without viscosity.

Figure 4 represents the movement of the particle using the SPH method (circles) in good agreement with the theoretical results (line) obtained from Eq. (21). The position and velocity are observed to be periodic. The particle trajectory in phase space follows a cycle. The collision is observed to be elastic. During most of the time, from 0 to A and from B to 0, the particle is under gravitational forces. Only from A to B the particle is under the force exerted from the boundary, verifying  $V_z(2h^-) = -V_z(2h^+)$ , where the superscripts - and + refer to before and after the collision. Thus, the particle apparently conserves the mechanical energy, showing a closed trajectory and bouncing in an elastic manner.

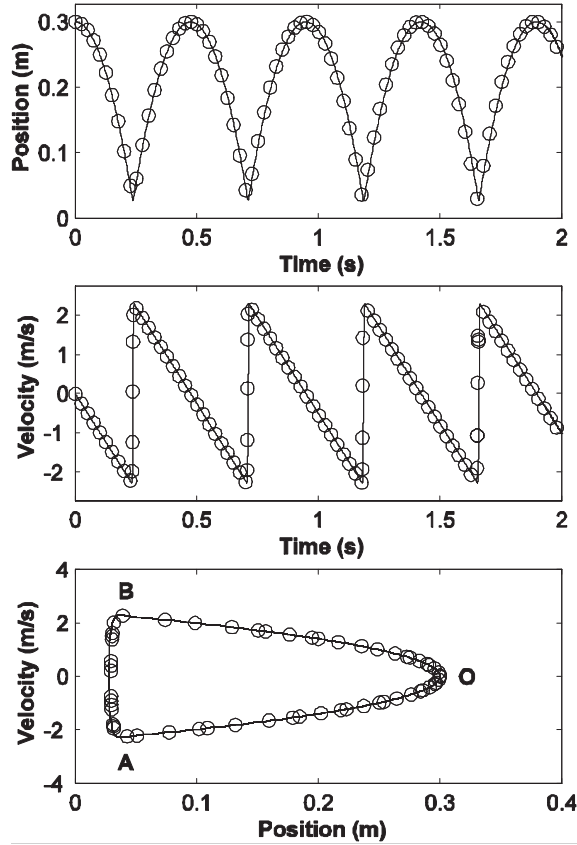


Figure 4: Single particle collision with a boundary in the absence of viscosity ( $\alpha=0$ ).

One of the main advantages of DBPs is the fact that boundary particles are considered a part of the system, in such a way that their energy can be calculated every time step to check energy evolution. To analyze energy conservation during the calculation the thermal energy associated to each particle is calculated using the expression given by Monaghan (1994)

$$\frac{du_a}{dt} = \frac{1}{2} \sum_b m_b \left( \frac{P_a}{\rho_a^2} + \frac{P_b}{\rho_b^2} + \Pi_{ab} \right) \vec{v}_{ab} \vec{\nabla}_a W_{ab} \quad (22)$$

The energy corresponding to the first collision between the moving particle and the boundary (Fig. 4) is depicted in Figure 5. Fluid particles energy evolution is represented in the left panel. Potential Energy (dashed line) decreases continuously until particle bounces. Kinetic Energy (dotted line) increases from the beginning of the ex-

periment and decreases sharply when the particle approaches to the tank bottom to increase in the same way after collision with the boundary. This rapid process corresponds to the inversion of velocity observed at the moment of the collision ( $t=0.24-0.25$  s). The Thermal energy of the fluid particle (solid line) increases at the moment of the collision although does not balance the decrease in kinetic energy. The remaining energy corresponds to changes in the thermal energy of the boundary. The total energy of fluid and boundary particles is represented in the right panel. First of all, the potential energy of the boundary particles was set to zero for the sake of clarity. Note that the potential energy of boundaries remains unchanged during the calculation and it can be considered as an offset. The energy of the moving particle (dotted line) decreases during the collision in an amount similar to the boundary energy increase (dashed line). This boundary energy is totally thermal since the boundary particles remain unchanged during the calculation. Instantaneous changes in the total energy (solid line), with a maximum increase around 1.5% of the total energy, are only observed during the collision. However, changes are balanced in such a way that the total energy of the system is exactly the same before and after the collision ( $E = 0.9196 J$ ).

To analyze the role of the viscosity on the fluid-boundary collision the same test depicted in Fig. 4 was carried out with  $\alpha=0.05$  (Fig.6). The line represents the theoretical prediction given by Eq. (21) and the circles represent the numerical results. Fig. 6 shows how the maximum height reached after each collision, decreases in time. This decrease can also be observed for velocity. The phase diagram shows an open trajectory due to the loss of mechanical energy of the fluid particle when approaching the boundary. Actually, one can observe how in a single collision  $V_z(2h^-) > V_z(2h^+)$ .

DBPs do not prevent wall penetration, which can be attained when the fluid particle approaches the boundary fast enough. The return point can be defined as the minimum distance from the incoming particle to the boundary divided by the smoothing length. The following numerical experiment was

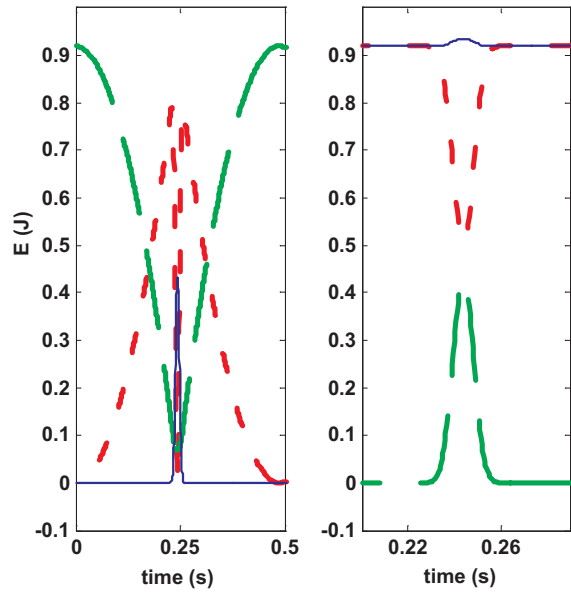


Figure 5: Energy of the fluid and boundary particles.

considered to analyze the dependence of the return point on the incident particle velocity. Once again, an inviscid medium ( $\alpha=0.0$ ) was considered. In addition, gravity was turned off in the model to assure a constant velocity, which was initially imposed to the incoming particle. Figure 7 shows the return point decrease when increasing the velocity of the incoming particle.

The inter-spacing between boundary particles can affect the repulsion force exerted by the wall. Actually, the *repulsive particles* method was refined in Monaghan and Kos (1999), by means of an interpolation process to minimize this effect. The dependence of the return point on inter-spacing should be checked in the *DBPs* method since there is not a specific mechanism to interpolate the exerted force. The calculation parameters previously described for Figure 7 were used in this case with an incoming velocity  $v_z=0.5 \text{ ms}^{-1}$ . The base configuration corresponds to the one shown in Figure 2, where the falling particle has the same  $X$  coordinate as the boundary particle. This configuration can be changed in  $X$  direction ( $\Delta x \in [-dx/2]$ ). The normalized return point was calculated using  $Z_n = z/z_0 * 100$ , where  $z$  is the return point for a certain  $\Delta x$  and  $z_0$  the return

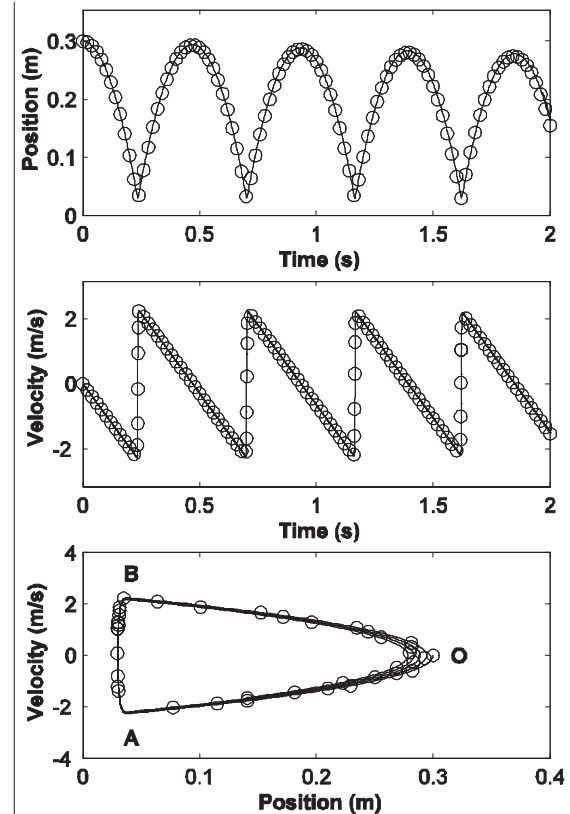


Figure 6: Single particle collision with a boundary in a viscous medium ( $\alpha=0.05$ ).

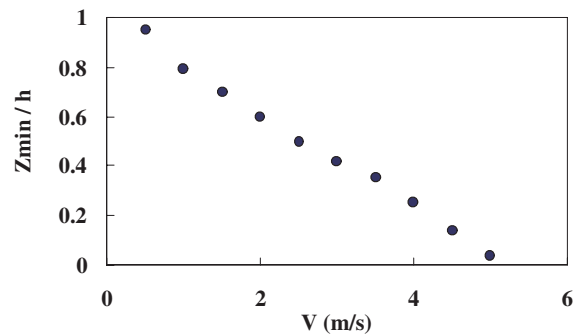


Figure 7: Return point for different incoming velocities of the moving particle.

point for  $\Delta x = 0$  (Figure 8). The return point is observed to decrease with  $\Delta x$  although variations from the case  $\Delta x=0$  are always lower than 0.1%. Obviously, the behavior is symmetric and only depends on  $\Delta x$ , not on the sign of the displacement from the base configuration.

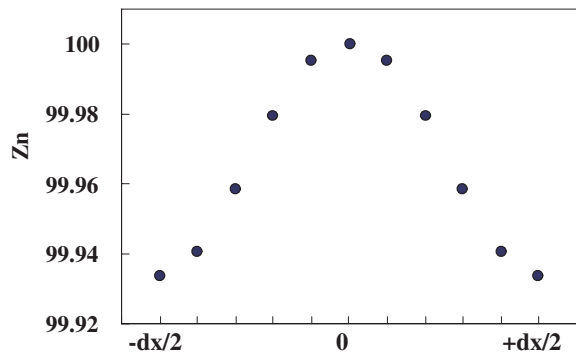


Figure 8: Dependence of the return point on the fall position.

### 3.3 Test problem 2: Collapse of a water column

Once the main properties of DBPs have been described in the previous oversimplified test case, DBPs will be used in a more realistic test. It consists in the collapse due to the gravity of a 2m high 2D water column in a tank. A complete description of the experiment is given by Koshizuka and Oka (1996) and a brief setup can be observed in Figure 9. The same setup was used by Violeau and Issa (2006) to check the accuracy of their SPH code. The tank is 4m long, the initial volume of water is 1m long and its height 2m. The number of boundary particles is 4,000 and the number of fluid particles is 40,000. A smoothing length,  $h=0.012$  m and a viscosity term,  $\alpha=0.5$ , were considered.

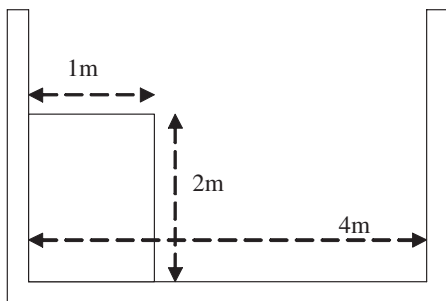


Figure 9: Initial configuration of the water column and the tank.

This laboratory test case will allow checking different properties of DBPs, namely, the fluid movement parallel to the left wall and bottom and

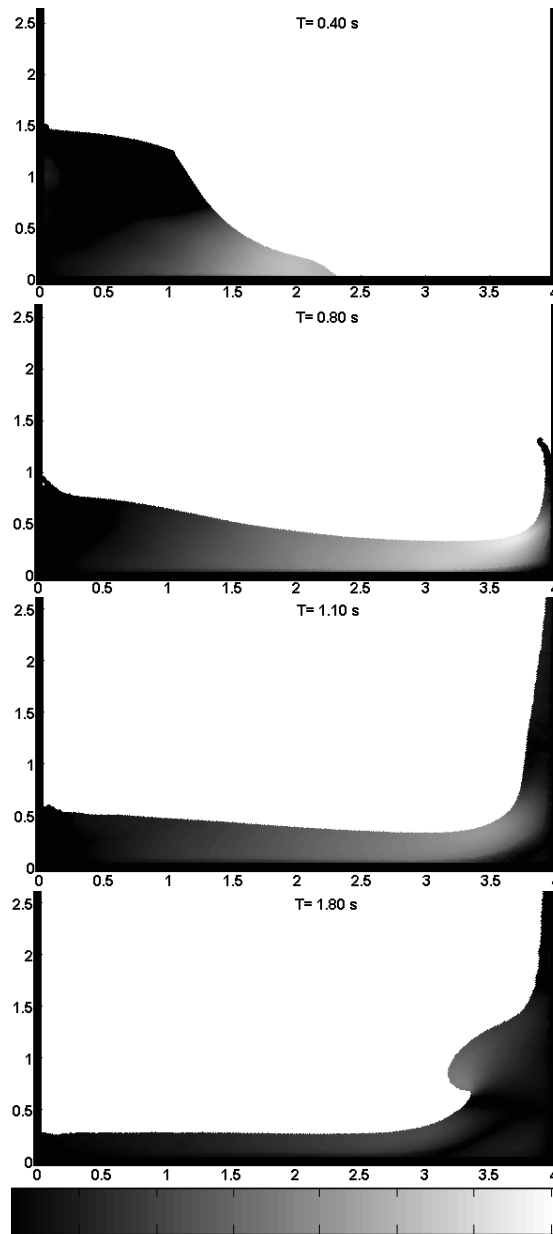


Figure 10: Collapse of a water column in a tank simulated with SPH model showing the particle velocities.

the fluid collision against the right wall.

On the one hand, the movement of the fluid inside the box depends on the interaction between the fluid and the boundary apart from the geometrical constraints of the initial water parcel. Thus, a proper boundary treatment will generate a realistic water height decrease near the left wall and

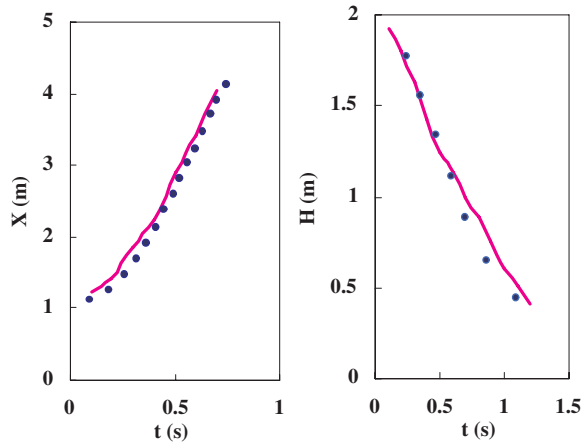


Figure 11: Collapse of a water column in a tank simulated with SPH model (solid line) comparing with experimental data (circles).

an accurate water velocity near the dam toe. On the other hand, the boundaries must prevent fluid escape through the right wall, which suffers the most energetic water collision in the experiment.

In the Figure 10, velocity magnitude ( $v = \sqrt{v_x^2 + v_z^2}$ ) is depicted at different instants of dam evolution. The colorbar is common to all snapshots. Distances are in meters and velocities in meters per second. Each particle is represented by a color corresponding to its instantaneous velocity. At  $T=0.4$ s the maximum dam break velocities are observed near the toe. The toe velocity evolution will be compared with experimental data in next figure. At  $T=0.8$ s the wave front has collided with the right wall. In  $T=1.1$ s water climbed onto the right wall. At  $T=1.8$ s water starts to fall over. The water height decrease near the left wall, which can be observed during the whole dam break, will also be compared to experimental data in Fig. 11.

As we mentioned above, an accurate water height ( $H$ ) decreases near the left wall and dam toe advance ( $X$ ) prove the proper behavior of boundary conditions. Fig. 11 shows how  $H$  and  $X$  fit data provided by Koshizuka and Oka (1996) experiment in an accurate way. Experimental points were digitalized from Violeau and Issa (2006).

## 4 Summary

Dynamic boundary particles (DBPs) have been considered to study the movement of fluid particles inside a container in the framework of a SPH method. These boundaries are constituted by fixed particles placed in a staggered grid manner and follow the same equations of state and continuity as the fluid particles. From the computational point of view, the treatment of the system is considerably simplified, since no special considerations are necessary for the boundary particles. In the looping over the particles they are simply marked with an index.

The validity of the method has been checked in an oversimplified geometry where a single particle impinges a boundary. The moving particle is observed to bounce due to the local increase of pressure terms in momentum equation. Thus, the boundaries retain the main features of the physical process: (a) they only exert a normal force on the fluid particles when approaching at a certain distance ( $r < 2h$ ); (b) the exerted force is almost independent of the particular position where the incident particle collides with the boundary; (c) the mechanical energy of the incident particle is conserved in absence of viscosity ( $\alpha = 0$ ).

The validity of the approach has also been checked in a dam break experiment. There, DBPs prevent fluid to leave the container and guarantee a proper water movement close to the walls.

Finally, DBPs can also be applied to mimic obstacles inside the computational domain and solid boundaries whose movement is externally imposed. In particular, DBPs have been used to generate wave mitigating dikes [Crespo, Gómez-Gesteira and Dalrymple (2007a)], sliding doors [Crespo, Gómez-Gesteira and Dalrymple (2007b)] and wavemakers [Crespo, Gómez-Gesteira and Dalrymple (2007c)].

**Acknowledgement:** This work was partially supported by Xunta de Galicia under the project PGIDIT06PXIB383285PR.

## References

- Batchelor G. K.** (1974): *Introduction to fluid dynamics*. Cambridge University Press.
- Benz W.** (1990): Smoothed particle hydrodynamics: A review in *The numerical Modelling of Non-linear Stellar Pulsations: Problems and Prospects*, J.R. Butcher ed., Kluwer Acad. Publ. 269-288
- Benz, W. and Asphaug, E.** (1994): Impact simulations with fracture. I. Methods and tests. *Icarus*, 107: 98-116.
- Benz W. and Asphaug, E.** (1995): Simulations of brittle solids using smoothed particle hydrodynamics. *Computational Physics Communications*, 87: 253-265.
- Bonet J. and Kulasegaram, S.** (2000): Corrections and stabilization of smooth particle hydrodynamics methods with applications in metal forming simulations. *International Journal for Numerical Methods In Engineering*, 47: 1189-1214.
- Crespo, A. J. C., Gómez-Gesteira, M. and Dalrymple, R.** (2007a): 3D SPH simulation of large waves mitigation with a dike. *Journal of Hydraulic Research*. In press.
- Crespo, A. J. C., Gómez-Gesteira, M. and Dalrymple, R.** (2007b): Modelling dam break behavior over a wet bed by an SPH technique. Submitted to *J. Wtrwy. Port, Coastal and Ocean Engrg.*
- Crespo, A. J. C., Gómez-Gesteira, M. and Dalrymple, R.** (2007c): Hybridation of generation propagation models and SPH model to study extreme wave events in Galician Coast. Submitted to *Journal of Marine Systems*.
- Dalrymple, R.A. and Knio, O.,** (2000): SPH Modelling of Water Waves. *Proc. Coastal Dynamics, Lund*, 779-787
- Dalrymple, R.A., Knio, O, Cox, D.T., Gómez-Gesteira, M., and Zou, S.** (2002): Using a Lagrangian particle method for deck overtopping. *Proceedings of Waves 2001*, ASCE. 1082-1091.
- Gingold, R. A. and Monaghan, J.J.** (1977): Smoothed particle hydrodynamics: theory and application to non-spherical stars, *Mon. Not. R. Astr. Soc.*, 181, 375- 389.
- Gómez-Gesteira and Dalrymple, R.** (2004): Using a 3D SPH Method for Wave Impact on a Tall Structure, *J. Wtrwy. Port, Coastal and Ocean Engrg.*, 130(2), 63-69.
- Gómez-Gesteira, M., Cerqueiro, D., Crespo, C., and Dalrymple, R.** (2005): Green water overtopping analyzed with a SPH model, *Ocean Engineering*, 32: 223-238.
- Koshizuka, S. and Oka, Y.** (1996): Moving-particle semi-implicit method for fragmentation of compressible fluid. *Nuclear Science Engineering*. 123, 421-434.
- Liu, G.R.** (2003): *Mesh Free methods: Moving beyond the finite element method*. CRC Press, pp. 692.
- Lucy, L.** (1977): A numerical approach to the testing of fusion process, *Journal Astronomical*, 82: 1013-1024.
- Monaghan, J. J.** (1982): Why particle methods work. *Siam J. Sci. Stat. Comput.*, 3: 422-433.
- Monaghan, J. J. and Latanzio, J.C.** (1985): A refined method for astrophysical problems. *Astron. Astrophys*, 149: 135- 143.
- Monaghan, J. J.** (1989): On the Problem of Penetration in Particle Methods. *Journal Computational Physics*, 82: 1-15.
- Monaghan, J. J.** (1992): Smoothed particle hydrodynamics. *Annual Rev. Astron. Appl.*, 30: 543- 574.
- Monaghan, J. J.** (1994): Simulating free surface flows with SPH. *Journal Computational Physics*, 110: 399- 406.
- Monaghan, J. J.** (1996): Gravity currents and solitary waves. *Physica D.*, 98: 523-533.
- Monaghan, J. J. and Kos, A.** (1999): Solitary Waves on a Cretan Beach. *J. Wtrwy. Port, Coastal and Ocean Engrg.*, 125: 145-154.
- Monaghan, J. J., Cas, R. F., Kos, A., and Hallworth, M.** (1999): Gravity currents descending a ramp in a stratified tank. *Journal Fluid Mechanics*, 379: 39-70.
- Monaghan, J. J.** (2000): SPH without Tensile Instability. *Journal Computational Physics*, 159: 290-311.
- Monaghan, J. J. and Kos, A.** (2000): Scott Rus-

sell's Wave Generator. *Physics of Fluids*, 12: 622-630.

**Peskin, C. S.**, (1977): Numerical analysis of blood flow in the heart. *Journal Computational Physics* 25, 220- 252.

**Randles, P.W. and Libersky, L.D.** (1996): Smoothed Particle Hydrodynamics – some recent improvements and applications. *Comput. Methods Appl. Mech. Eng.*, 138, 375- 408.

**Verlet, L.** (1967): Computer Experiments on Classical Fluids. I. Thermodynamical Properties of Lennard-Jones Molecules. *Phys. Rev.* 159, 98-103.

**Vignjevic, R., De Vuyst, T. and Campbell, J. C.** (2006): A Frictionless Contact Algorithm for Meshless Methods. *CMES: Computer Modeling in Engineering & Sciences*. 13 (1), 35-47.

**Vignjevic, R., Reveles, J. R. and Campbell, J. C.** (2006): SPH in a Total Lagrangian Formalism. *CMES: Computer Modeling in Engineering & Sciences*. 14 (3), 181-198.

**Violeau, D. and Issa, R.** (2006): Numerical Modelling of Complex Turbulent Free-Surface Flows with the SPH Method: an Overview. *Int. J. Numer. Meth. Fluids* 53, 277-304.